Supporting Information

Biomass-derived Porous carbon anchoring $MnFe_2O_4$ Hollow sphere and needle-like NiS for Flexible All-Solid-State Asymmetric Supercapacitor.

*Priyanka Makkar[a], Ankur Malik[b] and Narendra Nath Ghosh[a]**

[a]Nano-materials Lab, Department of Chemistry, Birla Institute of Technology and Science, Pilani K K Birla Goa Campus, Goa-403726, India.

[b]Department of Chemistry, Indian Institute of Technology, Roorkee, India

*Corresponding author. Tel. /fax: +91 832 2580318/25570339.

*E-mail address: naren70@yahoo.com (N. N. Ghosh)

2.1. Synthesis of activated porous carbon from coconut fiber. The synthesis of biomass-derived porous carbon from coconut fibers is a two-step process. In the first step, the 2 g of coconut fibers were treated hydrothermally by dispersing in 50 ml of 1 M H_2SO_4 solution. The solution is transferred to a 60 ml hydrothermal Teflon container for pretreatment at 200 ˚C for 24 hrs. After pretreatment, the fibers were cooled to room temperature naturally followed by filtration and washing several times with DI water. The fibers were dried at 70 ˚C overnight. In the second step, the pretreated coconut fibers were chemically activated using KOH (1:1 ratio of coconut fibers and KOH). And heated at 900 ˚C for 3 h in a nitrogen atmosphere. After cooling to room temperature, the product was washed with DI water. Finally, the product was dried in an oven at 70 ˚C for 12 hr.

Synthesis of $MnFe_2O_4$ hollow sphere. The $MnFe_2O_4$ hollow spheres are synthesized by the hydrothermal technique.[1] The salts of $MnCl_2 \cdot 4H_2O$ and $FeCl_3 \cdot 6H_2O$ (molar ratio 1:2) were dissolved in ethylene glycol followed by the addition of sodium acetate (NaAc) and poly(ethylene glycol) (PEG) (weight ratio 1:3.6) The mixture was stirred vigorously for 30 min until the dissolution of NaAc and PEG occurred completely. Then the reaction mixture was poured into a Teflon-lined stainless-steel autoclave for heating at 200 ˚C for 22 h. Then the precipitate was collected from the reaction mixture by the external magnet, followed by thorough washing with distilled water, ethanol, and acetone. The precipitate was dried at 60 ˚C for overnight.

Synthesis of Needle-shaped NiS. Needle-shaped NiS was synthesized by a two-step synthesis methodology.[2] Firstly, the green-colored $Ni(OH)_2$ precursor was synthesized by dissolving 0.872 g of $Ni(NO_3)_2 6H_2O$ and 0.364 g of urea in 40 mL of deionized water under vigorous stirring to obtain a pale green solution. Then, 0.012 g tri-sodium citrate was added to the resulting dispersion. After stirring for 30 min, the resulting solution was transferred into a 50 mL Teflon-lined stainless autoclave and kept at 150 ˚C for 24 h. The green precipitates were collected followed by washing with deionized water and

absolute ethanol several times by centrifugation. The collected precipitate was dried at 60 ˚C for 8 h. In the second step, the 0.106 g of the obtained green precursor was dispersed into 40 mL of absolute ethanol followed by the addition of 0.228 g of thiourea. After thorough stirring for 5 min, the mixed solution was transferred into a 50 mL Teflon lined stainless autoclave and heated at 120 °C for 24 h. The black precipitates were collected by centrifugation, washed with deionized water and absolute ethanol several times, and dried under 60 ˚C for 8 h.

Chemicals required. Sodium nitrate ($NaNO_3$), hydrazine hydrated ($N_2H_4.H_2O$), polyvinylpyrrolidone (PVP), sodium hydroxide (NaOH), polyvinyl alcohol (PVA), acetone, Ethanol, sodium acetate (NaAc), nickel(II) chloride hexahydrate ($NiCl_2.6H_2O$), and sulphuric acid (H_2SO_4), were procured from Fischer Scientific. Ethylene glycol was purchased from Merck, India. Manganese chloride tetrahydrate ($MnCl_2.4H_2O$), iron chloride hexahydrate ($FeCl_3.6H_2O$), potassium hydroxide, and polyethylene glycol (PEG) were purchased from Molychem. N-methyl-2-pyrrolidinone (NMP) was purchased from Sigma Aldrich.

2.2. Characterization. The in-depth characterization of the synthesized nanocomposite, room temperature powder X-ray diffraction (XRD) patterns of the synthesized materials were recorded using a powder X-ray diffractometer (Mini Flex II, Rigaku, Japan) with Cu Kα (λ = 0.15405 nm) radiation at a scanning speed of 3˚ min^{-1}. Raman spectra were recorded on a Horiba via Raman microscope with a 633 nm laser excitation, the surface area of the porous carbon was calculated by Bruner-Emmett-Teller (BET) N_2 adsorption-desorption isotherms, Field emission scanning electron microscopy (FESEM) images of samples were obtained using Quanta 250 FEG (FEI), and Energy-dispersive X-ray spectra (EDS) of the synthesized material was recorded using an EDAX ELEMENT electron microscope, X-ray photoelectron spectra (XPS) of the synthesized materials were recorded using PHI 5000 Versa Probe III,

Physical Electronics. IVIUMSTAT (10V/5A/8MHz) workstation was used to perform the electrochemical studies.

2.3. Electrochemical Measurements. In the present study, the electrochemical properties of the synthesized materials were investigated by assembling the three-electrode cell. Here, to fabricate the working electrodes, pure PC, $MnFe_2O_4$, $MnFe_2O_4$-PC, and $MnFe_2O_4$-NiS-PC nanocomposites were used as active materials. First, a viscous paste was prepared by mixing 80 wt% of active material, 10 wt% polyvinylidene difluoride in N-methyl-2-pyrrolidinone, and 10 wt% acetylene black. The working electrode was fabricated by loading ~ 2 mg of this paste on Ni foam with the dimension of (1.5 cm × 1.5 cm × 0.2 mm) and then dried at 80 ˚C for 12 h under vacuum. In the three-electrode system, a Hg/HgO electrode and a Pt wire were used as the reference electrode and the counter electrode, respectively. Electrochemical measurements were conducted using two electrolytes (i) 3 M KOH aqueous solution, and (ii) an aqueous mixture of 3 M KOH and 0.1 M $K_4[Fe(CN)_6]$.

2.3.1. Design of Asymmetric Device. The voltammetric charges (Q) were calculated based on the following equations:

$$Q = C_{single} \times \Delta V \times m \quad \text{(S1)}$$

where m is the mass of the electrode (g), ΔV is the potential window (V), and C_{single} is the specific capacitance (F g^{-1}) of each electrode measured in a three-electrode setup (calculated from cyclic voltammograms at a scan rate of 10 mV s^{-1}).

Balancing of charge is carried out by substituting the above equation for both anode and cathode considering their charge/mass ratio as:

$$\frac{q_+}{q_-} = \frac{m_+}{m_-} = \frac{C_{sp-} \times \Delta V^-}{C_{sp+} \times \Delta V^+} \quad \text{(S2)}$$

Equations:

Three-electrode Setup

The values of C_s, energy density (E), and power density (P) for a three-electrode setup was determined by using the following equations:

$$C_s = \frac{i\Delta t}{m\Delta V} \quad \text{(S3)}$$

$$E = \frac{C_s \times (\Delta V)^2}{2} \quad \text{(S4)}$$

$$P = \frac{E}{\Delta t} \quad \text{(S5)}$$

where C_s is the specific capacitance based on the mass of the electroactive material (F g^{-1}), i (A) represents the charge or discharge current, Δt (s) is the discharge time, m (g) represents the mass of supercapacitive material and ΔV is the applied potential window, E is the average energy density (Wh kg^{-1}), P is the power density (W kg^{-1}), and Δt is the discharge time (s).

Two-electrode Asymmetric Cell

The values of C_s, energy density (E), and power density (P) for two-electrode asymmetric setup was determined by using the following equations:

$$C_s = \frac{i\Delta t}{m\Delta V} \quad \text{(S6)}$$

$$E = \frac{C_s \times (\Delta V)^2}{2} \quad \text{(S7)}$$

$$P = \frac{E}{\Delta t} \quad \text{(S8)}$$

where C_s is the specific capacitance based on the mass of the electroactive material (F g^{-1}), i (A) represents the charge or discharge current, Δt (s) is the discharge time, m (g) represents the mass of supercapacitive material and ΔV is the applied potential window, E is the average energy density (Wh kg^{-1}), P is the power density (W kg^{-1}), and Δt is the discharge time (s).

Coulombic Efficiency

$$\% \text{ coulombic efficiency} = \frac{n_{td}}{n_{tc}} \times 100 \qquad \text{(S9)}$$

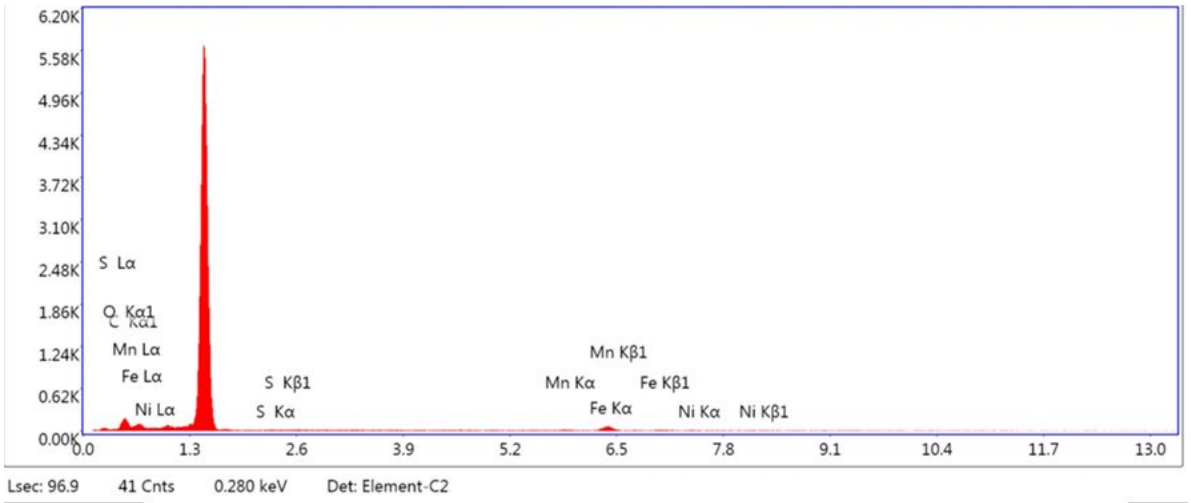

Element	Weight %	Atomic %	Net Int.
C K	18.4	31.0	4.0
O K	43.6	55.1	19.9
S K	0.8	0.5	0.8
MnK	5.7	2.1	2.5
FeK	25.2	9.1	9.4
NiK	6.3	2.2	1.8

Figure S1. EDS spectra of synthesized $MnFe_2O_4$-NiS-PC nanocomposite.

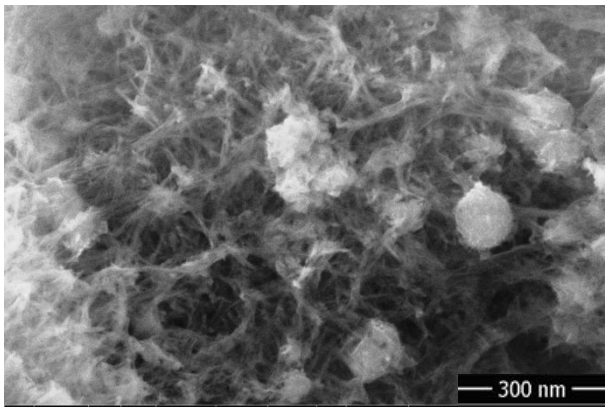

Figure S2. FESEM micrograph of needle-shaped NiS.

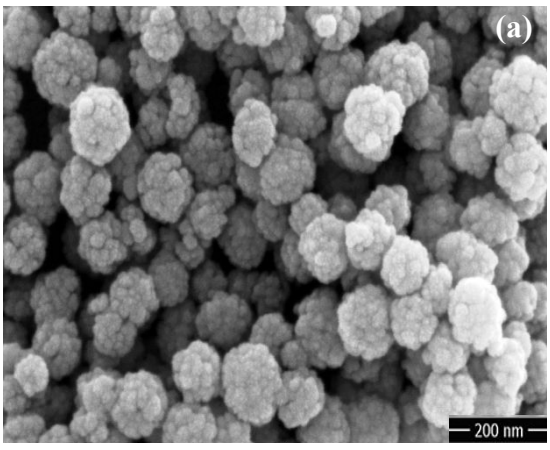

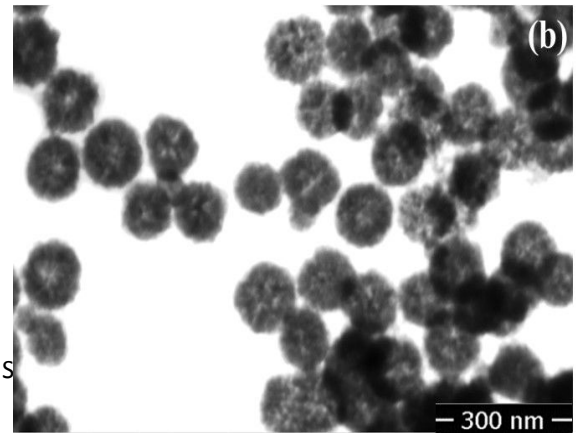

Figure S3. (a) FESEM micrograph of $MnFe_2O_4$ hollow spheres, (b) STEM detector-captured images of $MnFe_2O_4$ hollow microsphere.

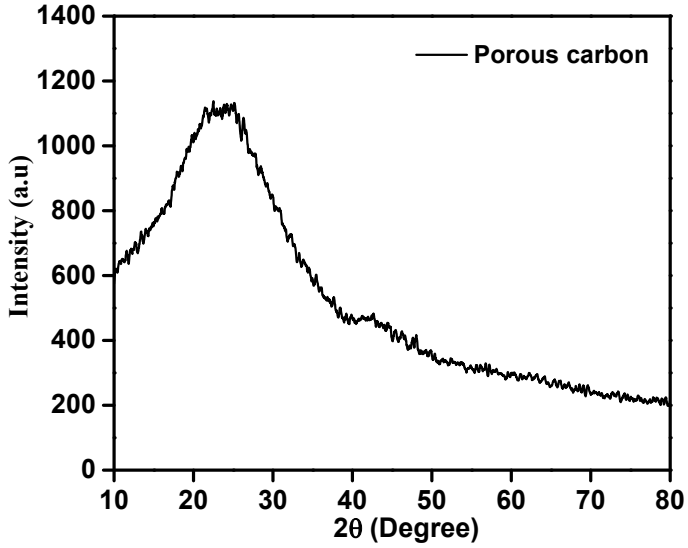

Figure S4. XRD pattern of pure PC.

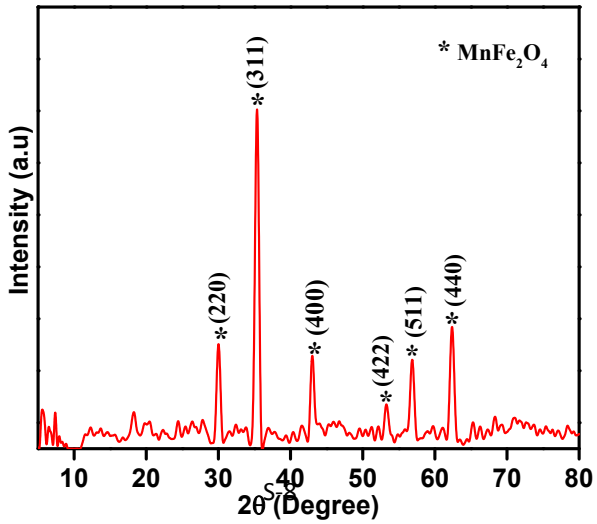

Figure S5. XRD pattern of pure $MnFe_2O_4$.

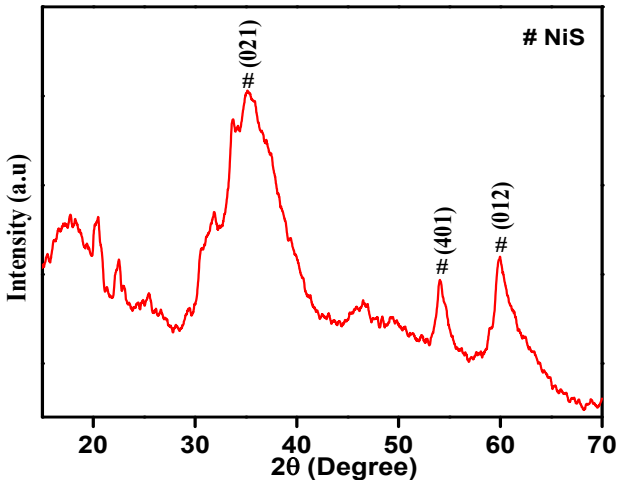

Figure S6. XRD pattern of pure NiS.

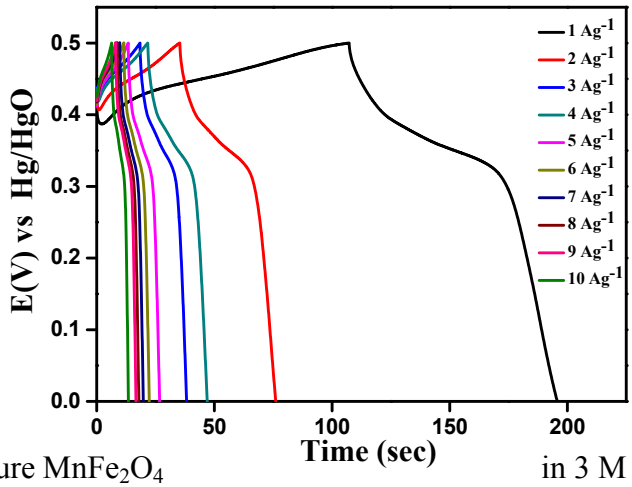

Figure S7. GCD curves of pure $MnFe_2O_4$ in 3 M KOH.

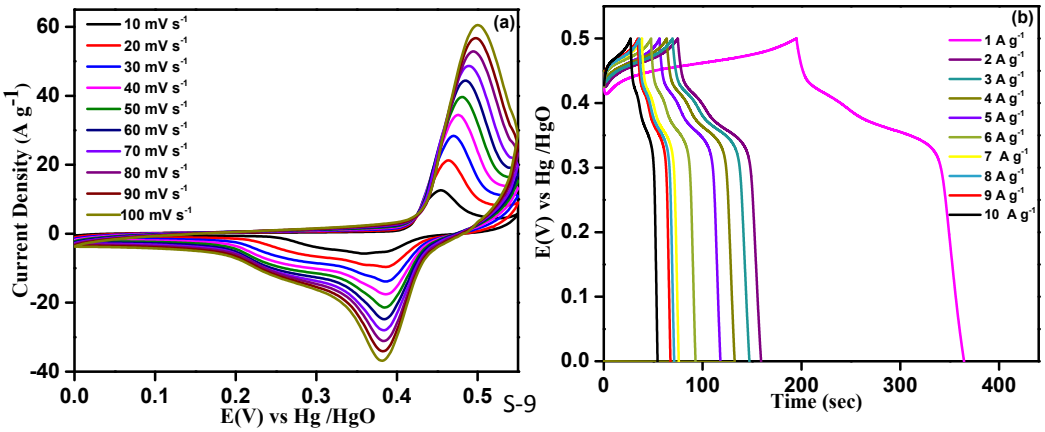

Figure S8. (a) CV profile at a scan rate of 10-100 mV s^{-1}. (b) GCD curves at current density varying from 1-10 A g^{-1} of $MnFe_2O_4$-PC electrode in 3 M KOH in three-electrode setup.

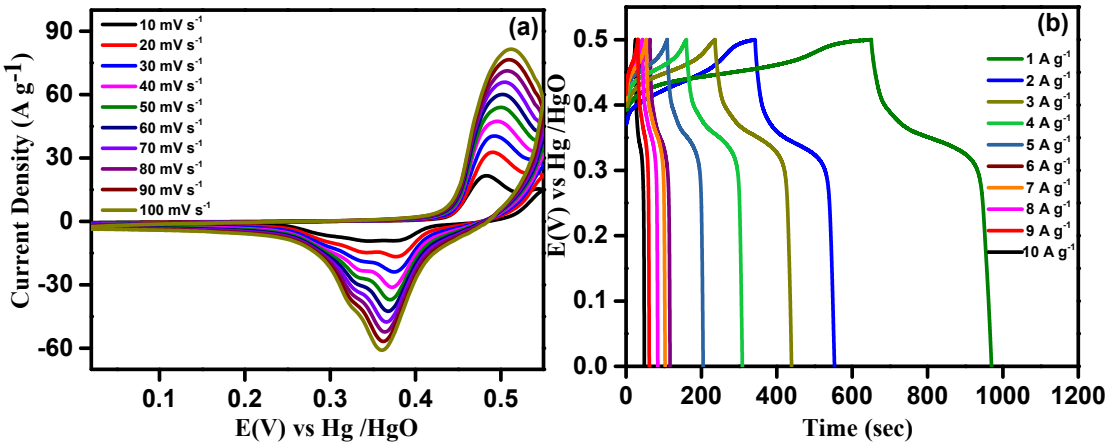

Figure S9. (a) CV curves, (b) GCD curves of $MnFe_2O_4$-NiS-PC in 3 M KOH in three-electrode setup.

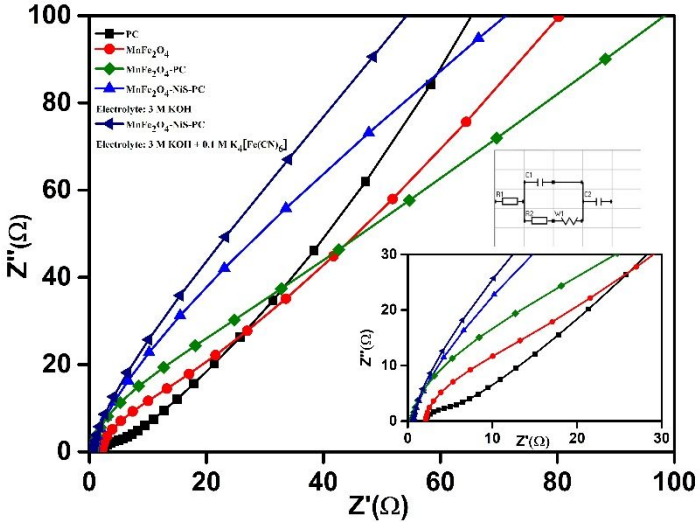

Figure S10. Nyquist plots of pure $MnFe_2O_4$, PC, $MnFe_2O_4$-PC and $MnFe_2O_4$-NiS-PC and inset shows the high frequency region of the impedance spectra and equivalent circuit used for fitting the Nyquist plots. All measurements are taken in three-electrode setup.

Table S1. Fitting results of the EIS data of synthesized nanocomposites in three-electrode setup.

S.No.	Material	Equivalent Series Resistance ($R_1 = R_S$) Ω	Charge Transfer Resistance ($R_2 = R_{ct}$) Ω	W1 (Warburg) Ω	$C_1 = C_{DL}$ (F)	$C_2 = C_{PS}$ (F)
1.	PC (3 M KOH)	2.39	2.56	2.95E-03	1.94E-03	1.00E-01
2.	$MnFe_2O_4$ (3 M KOH)	2.12	10.13	1.04E-02	6.43E-05	2.09E-02
3.	$MnFe_2O_4$-PC (3 M KOH)	1.86	2.07	3.51E-02	1.19E-03	5.67E-02
4.	$MnFe_2O_4$-NiS-PC (3 M KOH)	1.51	1.82	4.83E-03	1.48E-03	2.36E-02
5.	$MnFe_2O_4$-NiS-PC (3 M KOH + 0.1 M $K_4[Fe(CN)_6]$	1.12	1.33	2.95E-03	1.94E-03	1.00E-01

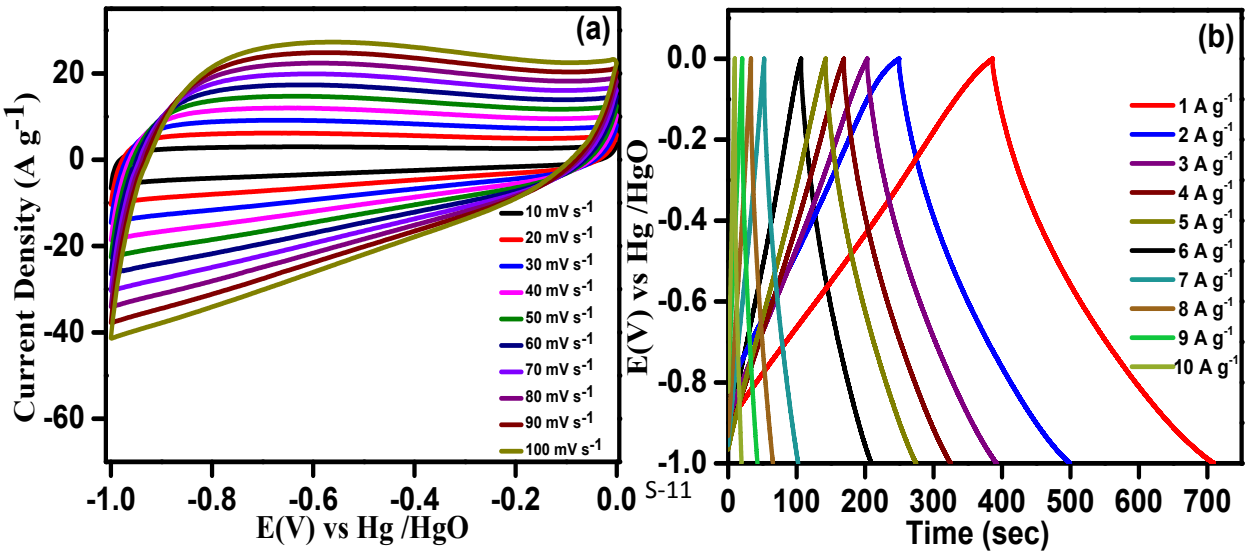

Figure S11. (a) CV curve, (b) GCD curves of porous carbon.

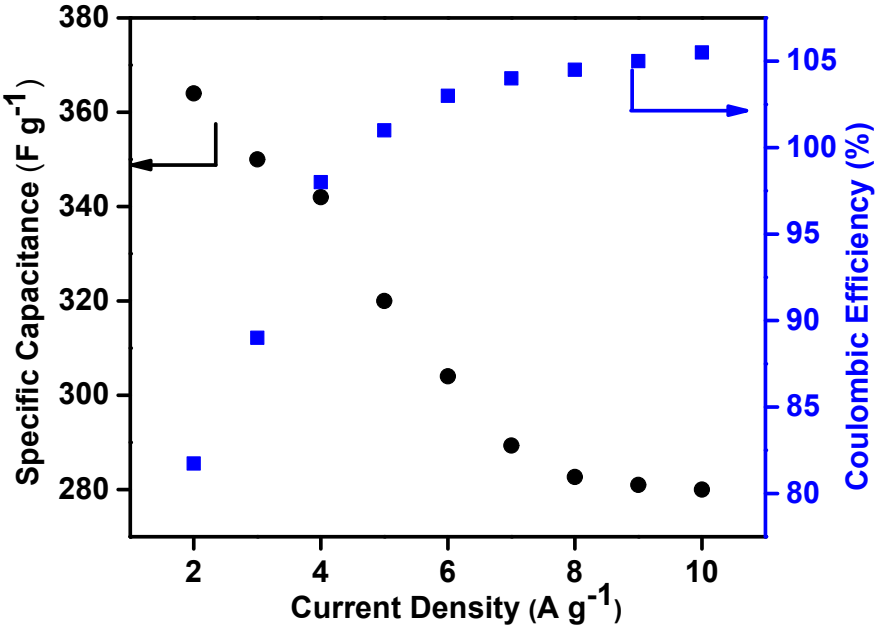

Figure S12. Variation of specific capacitance and Coulombic efficiency with changing current density.

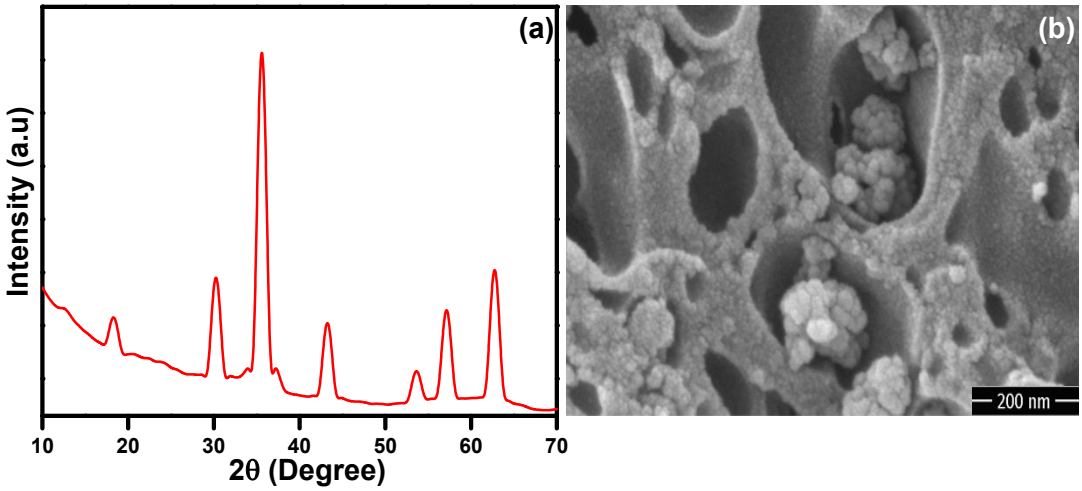

Figure S13. (a) XRD pattern and (b) FESEM micrograph of the $MnFe_2O_4$-NiS-PC//PC device electrode after charge-discharge cycles

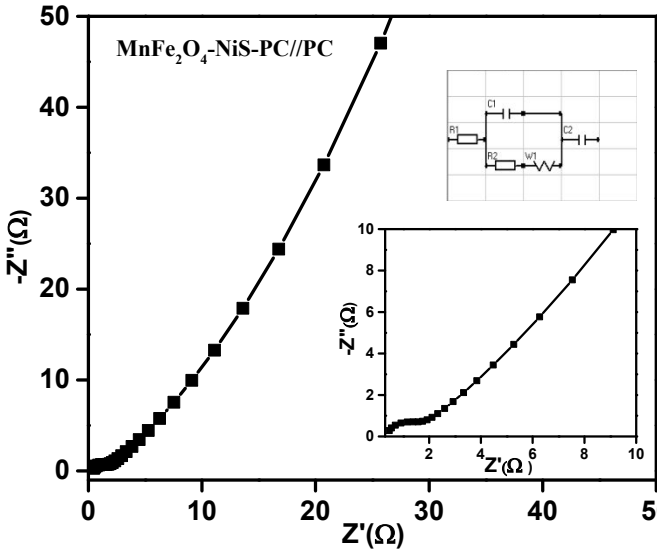

Figure S14. Nyquist plot of $MnFe_2O_4$-NiS-PC//PC device and inset shows the high-frequency region of the impedance spectra and equivalent circuit used for fitting the Nyquist plots.

Table S2. Fitting results of the EIS data of all-solid-state flexible asymmetric $MnFe_2O_4$-NiS-PC//PC device supercapacitor device

Equivalent Series Resistance ($R_1 = R_s$) Ω	Charge Transfer Resistance ($R_2 = R_{ct}$) Ω	W1 (Warburg) Ω	C1 = C_{DL} (F)	C2 = C_{PS} (F)
0.39	1.1	5.81E-02	2.08E-04	1.76E-01

Two-electrode Asymmetric Cell

The values of C_s, energy density (E), and power density (P) for two-electrode asymmetric setup was determined by using the following equations:

$$C_s = \frac{i\Delta t}{m\Delta V} \quad \text{(S10)}$$

$$E = \frac{C_s \times (\Delta V)^2}{2} \quad \text{(S11)}$$

$$P = \frac{E}{\Delta t} \quad \text{(S12)}$$

where C_s is the specific capacitance based on the mass of the electroactive material (F g^{-1}), i (A) represents the charge or discharge current, Δt (s) is the discharge time, m (g) represents the mass of supercapacitive material and ΔV is the applied potential window, E is the average energy density (Wh kg^{-1}), P is the power density (W kg^{-1}), and Δt is the discharge time (s).

Table S3. Comparison of electrochemical performance of some two-electrode asymmetric supercapacitor devices.

S.No.	Material	Electrolyte	Working Potential (V)	Power Density (W kg^{-1})	Energy Density (Wh kg^{-1})	Retention	Reference
1)	$ZnFe_2O_4$// NRG composite	1 M KOH	-1 to 0	3000	6.7	84.4% (1000cycles)	**3**
2)	$MnFe_2O_4$//	1 M Na_2SO_4	0 to 1.8	900	25.9	90%	**4**

	Graphene					(4000 cycles)	
3)	Ni-Co oxide//AC	1 M KOH	-1 to 0	270	8.9	85% (2000 cycles)	**5**
4)	CuO//AC	3 M KOH	0 to 1.4	700	19.7	96% (3000 cycles)	**6**
5)	NiO//carbon	6 M KOH	0 to 1.3	-	10	74% (1000 cycles)	**7**
6)	Carbon spheres/ MnO_2// carbon spheres	0.1 M Na_2SO_4	0 to 2	100	22.1	99% (1000 cycles)	**8**
7)	$NiCo_2O_4$-MnO_2/GF// CNT/GF	6 M KOH	0 to 1.5	187.5	55.1	89.4% (2000 cycles)	**9**
8)	Co_3O_4@ $NiCo_2O_4$ //AC	1 M KOH	0 to 1.6	852	36	89.5% (10000 cycles)	**10**
9)	ZnS Ni_7S_6/Ni(OH_2/ /NSGNs	5 M KOH	0 to 1.5	700.16	68.85	91.79% (10000)	**11**
10)	CoS//AC	3.5 M KOH	0 to1.8	1800	5.3	92% (5000 cycles)	**12**
11)	NiS_2/CoS_2/ NC-500//AC	3 M KOH	0 to1.6	800	53.93	85.71% (20000 cycles)	**13**
12)	Co_3O_4@CoNi S//NOPC	-	0 to 1.6	400	46.95	95.6% (20000	**14**

13)	Co_3O_4 NSs-rGO//AC	2 M KOH	0 to 1.45	2166	13.4	89% (1000 cycles)	**15**
14)	NiS//AC	3 M KOH	0 to 1.8	900	31	100% (1000 cycles)	**16**
15)	ZnS/Ni_3S_2// AC	3 M KOH	0 to 1.7	849.4	51.2	71% (6000 cycles)	**17**
16)	NiS//CNFs	2 M KOH	0 to 1.55	387.5	34.9	90.2% (3000 cycles)	**18**
17)	$NiFe_2Se_4$//AC	3 M KOH	0 to 1.6	800	45.6	101.4% (10000 cycles)	**19**
18)	80$MnFe_2O_4$-20rGO//rGO	3 M KOH + 0.1 M $K_4[Fe(CN)_6]$	0 to 1.5	750	27.7	95% (4000 cycles)	**2**
19)	$MnFe_2O_4$-NiS-PC// PC	3 M KOH + 0.1 M $K_4[Fe(CN)_6]$	0 to 1.5	1500	113	98% (10000 cycles)	**This work**

REFERENCES

1. Guan, B.; Li, Y.; Yin, B.; Liu, K.; Wang, D.; Zhang, H.; Cheng, C. Synthesis of hierarchical NiS micro flowers for high-performance asymmetric supercapacitor. *Chem. Eng. J.* **2017**, *308*, 1165-1173.

2. Makkar, P.; Ghosh, N. N. Facile Synthesis of $MnFe_2O_4$ Hollow Sphere-Reduced Graphene Oxide Nanocomposites as Electrode Materials for All-Solid-State Flexible High-Performance Asymmetric Supercapacitors. *ACS Appl. Energy Mater*. **2020**, *3*, 2653-2664.

3. Li, L.; Bi, H.; Gai, S.; He, F.; Gao, P.; Dai, Y.; Zhang, X.; Yang, D.; Zhang, M.; Yang, P. Uniformly dispersed $ZnFe_2O_4$ nanoparticles on nitrogen-modified graphene for high-performance Supercapacitor as Electrode. *Sci Rep.* **2017**, *7*, 43116.

4. Li, B.; Fu, Y.; Xia, H.; Wang, X. High-performance asymmetric supercapacitors based on $MnFe_2O_4$/graphene nanocomposite as anode material. *Mater. Lett.* **2014**, *122*, 193-196.

5. Tang, C.; Tang, Z.; Gong, H. Hierarchically porous Ni-Co oxide for high reversibility asymmetric full-cell supercapacitors. *J. Electrochem. Soc.* **2012**, *159*, A651-A656.

6. Moosavifard, S. E.; El-Kady, M. F.; Rahmanifar, M. S.; Kaner, R. B.; Mousavi, M. F. Designing 3D highly ordered nanoporous CuO electrodes for high-performance asymmetric supercapacitors. *ACS Appl. Mater. Interfaces* **2015**, *7*, 4851-4860.

7. Wang, D.-W.; Li, F.; Cheng, H.-M. Hierarchical porous nickel oxide and carbon as electrode materials for asymmetric supercapacitor. *J. Power Sources* **2008**, *185*, 1563-1568.

8. Lei, Z.; Zhang, J.; Zhao, X. Ultrathin MnO_2 nanofibers grown on graphitic carbon spheres as high-performance asymmetric supercapacitor electrodes. *J. Mater. Chem*. **2012**, *22*, 153-160.

9. Garakani, M.A.; Abouali, S.; Xu, Z.L.; Huang, J.; Huang, J.Q.; Kim, J. K.. Heterogeneous, mesoporous $NiCo_2O_4$-MnO_2/graphene foam for asymmetric supercapacitors with ultrahigh specific energies. *J. Mater. Chem. A*. **2017**, *5*, 3547-3557.

10. Tao, K.; Yang, Y.; Yang, C.; Ma, Q.; Han, L. Construction of $NiCo_2O_4$ nanosheet-decorated leaf-like Co_3O_4 nanoarrays from metal-organic framework for high-performance hybrid supercapacitors. *Dalton Trans*. **2019**, *48*, 14156-14163.

11. Saeed, G.; Bandyopadhyay, P.; Kumar, S.; Kim, N.H.; Lee, J.H. ZnS-Ni_7S_6 Nanosheet Arrays Wrapped with Nanopetals of $Ni(OH)_2$ as a Novel Core-Shell Electrode Material for Asymmetric

Supercapacitors with High Energy Density and Cycling Stability Performance, *ACS Appl. Mater. Interfaces* **2020**, *12*, 47377-47388.

12. Subramani, K.; Sudhan, N.; Divya, R.; Sathish. M. All-solid-state asymmetric supercapacitors based on cobalt hexacyanoferrate-derived CoS and activated carbon. *RSC Adv*. **2017**, *7*, 6648-6659.

13. Liu, H.; Guo, H.; Yue, L.; Wu, N.; Li, Q.; Yao, W.; Xue, R.; Wang, M.; Yang, W. Metal-organic frameworks-derived NiS_2/CoS_2/N-doped carbon composites as electrode materials for asymmetric supercapacitor. *ChemElectroChem*. **2019**, *6*, 3764-3773.

14. Yan, Y.; Ding, S.; Zhou, X.; Hu, Q.; Feng, Y.; Zheng, Q.; Lin, D.; Wei, X.. Controllable preparation of core-shell Co_3O_4@CoNiS nanowires for ultra-long life asymmetric supercapacitors. *J. Alloys and Compd.* **2021**, *867*, 158941

15. Yuan, C.; Zhang, L.; Hou, L.; Pang, G.; Oh, W.-C. One-step hydrothermal fabrication of strongly coupled Co_3O_4 nanosheets-reduced graphene oxide for electrochemical capacitors. *RSC Adv.* **2014**, *428*, 14408-14413.

16. Guan, B.; Li, Y.; Yin, B.; Liu, K.; Wang, D.; Zhang, H.; Cheng, C. Synthesis of hierarchical NiS microflowers for high performance asymmetric supercapacitor. *Chem. Eng. J.* **2017**, *308*, 1165-1173.

17. Zhang, Y.; Cao, N.; Li, M.; Szunerits, S.; Addad, A.; Roussel, P.; Boukherroub, R.. Self-template synthesis of ZnS/Ni_3S_2 as advanced electrode material for hybrid supercapacitors. *Electrochim. Acta* **2019**, *328*, 135065.

18. Ma, X.; Zhang, L.; Xu, G.; Zhang, C.; Song, H.; He, Y.; Zhang, C.; Jia, D. Facile synthesis of NiS hierarchical hollow cubes via Ni formate frameworks for high-performance supercapacitors. *Chem. Eng. J*. **2017**, *320*, 22-28.

19. Ye, B.; Cao, X.; Zhao, Q; Wang, J. Electrodeposited $NiFe_2Se_4$ on Nickel Foam as a Binder-Free Electrode for High-Performance Asymmetric Supercapacitors. *Ind. Eng. Chem. Res*. **2020**, *59*, 14163-14171.